ALTERNATIVE ADSORBENT MATERIALS FOR APPLICATION IN INDUSTRIAL PROCESSES

CrossMark

Amino-Fe$_3$O$_4$-functionalized graphene oxide as a novel adsorbent of Methylene Blue: kinetics, equilibrium, and recyclability aspects

Tiago José Marques Fraga[1] · Letticia Emely Maria de Lima[2] · Ziani Santana Bandeira de Souza[1] ·
Marilda Nascimento Carvalho[1] · Eleonora Maria Pereira de Luna Freire[1] · Marcos Gomes Ghislandi[3] ·
Maurício Alves da Motta[1]

Abstract

Graphene oxide (GO) was synthetized from graphite oxidation via the modified Hummers method. Afterwards, the GO was functionalized with diethylenetriamine (DETA) and FeCl$_3$ to obtain the novel amino-iron oxide functionalized graphene (GO-NH$_2$-Fe$_3$O$_4$). FTIR, XRD, SEM with EDX, and Raman spectroscopy were performed to characterize both GO and GO-NH$_2$-Fe$_3$O$_4$. The GO-NH$_2$-Fe$_3$O$_4$ was then evaluated as adsorbent of the cationic dye Methylene Blue (MB); analysis of the point of zero net charge (pH$_{PZC}$) and pH effect showed that the GO-NH$_2$-Fe$_3$O$_4$ pH$_{PZC}$ was 8.2; hence, the MB adsorption was higher at pH 12.0. Adsorption kinetics studies indicated that the system reached the equilibrium state after 5 min, with adsorption capacity at equilibrium (q_e) and kinetic constant (k_S) of 966.39 mg g^{-1} and 3.17·10^{-2} g mg^{-1} min^{-1}, respectively; moreover, the pseudo-second-order model was better fitted to the experimental data. Equilibrium studies showed maximum adsorption capacity of 1047.81 mg g^{-1}; furthermore, Langmuir isotherm better fitted the adsorption. Recycling experiments showed that the GO-NH$_2$-Fe$_3$O$_4$ maintained the MB removal rate above 95% after 10 cycles. All the results showed sorbent high adsorption capacity and outstanding regeneration capability and evidenced the employment of novel GO-NH$_2$-Fe$_3$O$_4$ as a profitable adsorbent of textile dyes.

Keywords Adsorption · Graphene oxide · Functionalization · Ecofriendly adsorbent · Textile effluent · Methylene Blue

Abbreviations
GO	Graphene oxide
GO-NH$_2$-Fe$_3$O$_4$	Amino-Fe$_3$O$_4$ functionalized graphene oxide
DETA	Diethylenetriamine
PTFE	Polytetrafluoroethylene
MB	Methylene Blue
PFO	Pseudo-first-order
PSO	Pseudo-second-order

✉ Tiago José Marques Fraga
tiago_mfraga@hotmail.com

Letticia Emely Maria de Lima
letticialima@gmail.com

Ziani Santana Bandeira de Souza
zianisbs@gmail.com

Marilda Nascimento Carvalho
marildacarv@gmail.com

Eleonora Maria Pereira de Luna Freire
eleonorafreire@yahoo.com.br

Marcos Gomes Ghislandi
marcos.ghislandi@ufrpe.br

Maurício Alves da Motta
mottas@ufpe.br

[1] Chemical Engineering Department, Federal University of Pernambuco (UFPE), 1235 Prof. Moraes Rego Avenue, Cidade Universitária, Recife, Pernambuco 50670-901, Brazil

[2] Center of Biosciences, Federal University of Pernambuco (UFPE), W/N Prof. Moraes Rego Avenue, Cidade Universitária, Recife, Pernambuco 50670-420, Brazil

[3] Engineering Campus – UACSA, Federal Rural University of Pernambuco (UFRPE), 300 Cento e sessenta e Três Av, Cabo de Santo Agostinho, Pernambuco, Brazil

⚫ Springer

Introduction

The textile industries generate a considerable environmental impact due to its elevated consumption of water, and high toxicity of their effluents. One fifth of the world's water pollution corresponds to dyes and other chemical species from the textile industry. Textile wastewaters are characterized as alkaline and with high biologic oxygen demand (BOD), between 700 and 3000 mgL^{-1}. Moreover, the salt concentration measured in real textile effluent varies between 2000 and 3000 mg L^{-1} (World Bank Group 2007). Besides being responsible for increasing biological oxygen demand (BOD), the lack of dissolved oxygen in water bodies to sustain aquatic life is reported as one of the consequence of dye release (Al-Qodah et al. 2007). When disposal occurs without due treatment, it results in severe environmental liabilities. Because of their persistence and toxicity, discarded dyes in water bodies have become a source of constant concern, as most of them are not biodegradable, reduce the penetration of light into water bodies, inhibiting algae photosynthesis, and tend to accumulate in living organisms (Hu et al. 2017; Al-Qodah et al. 2007). Their capacity to degrade into aromatic compounds makes them carcinogenic, mutagenic, and with inhibitory properties, causing damages not only in aquatic animals but also in humans, even at low concentrations (Yusuf et al. 2015). Between the diseases and other harms to human health caused by dyes, it can be cited hypersensitivity, dermatitis, cancer, skin irritation, dysfunction of kidneys, liver, and reproductive system (Shaban et al. 2018). Dye removal process by adsorption is a tertiary treatment, since it is usually used after processes such as filtration, aeration, biodigestion, and flocculation, among others. In this scenario, many researchers have been focusing on methods to treat effluents from the textile industry, having as object of study the development of low-cost materials and composites with good adsorptive capacity. Among these, nanomaterials derived from carbon have occupied a prominent place in recent research, and exfoliated graphene oxide nanosheets have been studied for its remarkable adsorptive properties (Araujo et al. 2018). In recent years, novel engineered nanosorbents reported in the literature have been successfully developed by doping, tailoring, active site activation, and the modification of functional groups over their surfaces aiming to enhance the adsorption efficiency towards several types of dyes (Bozorgi et al. 2018).

Carbon atoms have the ability to make covalent bonds along with the sp2 hybridized states, giving its structures the ability to overcome the metallic and non-metallic compounds. The flexibility of carbon structures is remarkable from the point of view of various geometric forms that can be obtained, such as nanotubes, nanosheets, nanohorns, and fullerenes, among others (Grima et al. 2015). Among these carbonaceous materials, graphene has attracted huge interest of several researchers worldwide due to its unique structural characteristics

and high adsorption performance. Carbon nanomaterials exhibit a unique combination of chemical and physical properties such as thermal and electrical conductivity, high mechanical strength, and optical properties (Cha et al. 2013), and related studies have increased in parallel with the development of transmission electron microscopy (Yang 2003). The precursor reported work of physical synthesis of graphene nanosheets with some purity is that performed by Novoselov et al. (2004), who used Scotch tape to separate the single graphene layers from the graphite crystals. Therefore, there has been a growing interest among the scientific community in investigating different aspects, particularly the surface modification, of graphene, such as functionalization, doping, and anchoring (Georgakilas et al. 2016; Kuila et al. 2012). Depending on the route, functionalization can enhance several graphene nanosheets properties, such as mechanical resistance, chemical selectiveness, electron, and thermic conductivity, between others (Georgakilas et al. 2016; Yusuf et al. 2015). In the environmental field, functionalized graphene-based nanomaterials have been widely employed as adsorbent of several water pollutants in recently reported works, which can be cited: metallic ions (Zhang et al. 2018), heavy metal (Lingamdinne et al. 2018), pharmaceuticals (Zhu et al. 2018), pesticides and herbicides (Lazarevic-Pasti et al. 2018; Wanjeri et al. 2018), crude oil and its derivatives (Diraki et al. 2018), volatile organic compounds (Yu et al. 2017), and dyes.

The objective of this work is developing a novel and high capable adsorbent for textile dyes; in that sense, it was evaluated the performance of the amino-Fe$_3$O$_4$-functionalized graphene oxide (GO-NH$_2$-Fe$_3$O$_4$) as adsorbent for the reference acid dye, Methylene Blue (MB). The kinetic and equilibrium parameters of MB adsorption were obtained and discussed, prior to further studies of the application of GO-NH$_2$-Fe$_3$O$_4$ as adsorbent of a larger variety of textile dyes. Moreover, recycling experiments were performed to evaluate the adsorbent regeneration capability. GO-NH$_2$-Fe$_3$O$_4$ adsorption efficiency was also extensively compared with other graphene-based nanomaterials employed as adsorbent of different species of dyes.

Materials and methods

Synthesis of GO

Graphene oxide (GO) was synthesized by the modified Hummers method (Araujo et al. 2018; Hummers and Offeman 1958). A 1.0 g of powdered graphite (Merck, 99%) was added along with 25 mL of H$_2$SO$_4$ 99% to a flask under stirring and rigorously controlled temperature below 12 °C until homogenization of the mixture. Then, 3.0 g of KMnO$_4$ was slowly added and the temperature set to 32 °C for a period of 6 h. After the graphite oxidation reaction, 35 mL of H$_2$O$_2$

30% was added to complete the oxidation; then, 200 mL of HCl 99% was added. Thereafter, the sample was successively washed with distilled water until the pH of the suspension was stabilized. After washing, the graphite oxide was submitted to sonication for 4 h to exfoliate the GO.

GO functionalization

An aliquot of 4.0 ml of GO suspension (~ 0.031 g mol^{-1}) was separated and mixed with 250 ml of monoethylene glycol, under heating to reach the temperature of 180 °C. Solvothermal method of anchoring magnetic Fe_3O_4 nanoparticles on GO nanosheets was performed by the addition of 0.5 g of $FeCl_3 \cdot 6H_2O$, 3.0 g of sodium acetate to GO suspension (Ai et al. 2011); moreover, 30 mL of diethylenetriamine (DETA) was added to the flasks to perform covalent amine functionalization of GO nanosheets simultaneously with Fe_3O_4 anchoring. Functionalization synthesis occurred in batch mode, in a 600-mL closed loop reflux reactor, with vigorous stirring speed for 6 h and temperature strictly controlled at 180 °C. Similar method was also employed by Zhao et al. (2016) to adsorb chromium ions from aqueous solution; however, the authors performed it at higher temperature and in a closed INOX reactor. After the reaction, the mixture was cooled to room temperature (24 °C), and subsequently washed with 150 mL of ethanol and washed successively with distilled water; the suspension was decanted and the supernatant was removed. GO nanosheets were magnetite-functionalized via non-covalent functionalization route; hence, Fe_3O_4 magnetic nanoparticles were linked to GO graphenic plane via interaction forces of small strength, such as Van der Waals forces and ionic interactions (Georgakilas et al. 2016; Yusuf et al. 2015; Kuila et al. 2012). Moreover, π-π stacking interactions also play a significant role on covalent and non-covalent functionalization due to wide π-electronic configuration formed over GO plane. Such interactions are associated at relatively lower levels of energies in comparison to dissociation energy of covalent single bonds (~ 350 kJ mol^{-1}) (Georgakilas et al. 2016). Thus, non-covalent functionalization of Fe_3O_4 occurred in parallel with the covalent functionalization of amine/amide groups over GO surface and edges. The functionalized GO suspension was then stocked to perform UV-vis scanning and subsequent characterization analyses, as well as for use in the adsorptive process.

Adsorbent characterization

The characterization of the graphite, GO, and the amino-Fe_3O_4-functionalized-GO was conducted by Fourier transformed infrared spectroscopy (FTIR), X-ray diffraction (XRD), scanning electron microscopy (SEM), and Raman spectroscopy. FTIR spectra of GO, GO-NH_2-Fe_3O_4, and GO-NH_2-Fe_3O_4 after 10 cycles of adsorption and desorption of MB were obtained by an infrared spectrometer model

Brucker Tensor 27 (Germany). XRD analyses were realized by using an X-ray diffractometer Rigaku Ultima (Japan). SEM analysis has been made using a Zeiss equipment, model LEO 440 (Germany), coupled with energy-dispersive X-ray (EDX) spectrometer. Finally, Raman spectra for graphite, GO, and GO-NH_2-Fe_3O_4 samples were obtained by a confocal Raman/AFM spectroscope model Witec Alpha 300 (Germany) (samples were irradiated with a 633 nm red laser). In each sample, three individual spectra were measured at random points; each spectrum was obtained with accumulations of 30 s using a lens of ×100 and a grid of 600 mm/line.

Batch sorption experiments

The samples of MB solution were transferred to flasks of 125 mL, and aliquots of OG-NH_2-Fe_3O_4 suspension were added. The samples were placed in a steering table for determined contact time. The adsorption experiments were conducted in batch, at the following conditions: 25 °C, 25 mL of adsorbate solution, agitation of 300 rpm, and solution pH 12.0, similar to reported textile effluent pH, measured after desizing, scouring, and mercerization process (Wang et al. 2011). Afterwards, the GO-NH_2-Fe_3O_4 was separated from the liquid phase by filtration in PTFE filters (45 μm).

The percentage of adsorbed dye in the GO-NH_2-Fe_3O_4 (dye removal efficiency, %) and the adsorption capacity (q, mg g^{-1}) were calculated using Eqs. 1 and 2:

$$\text{Percentage removal} : (\%) = \frac{C_0 - C}{C_0} \times 100 \tag{1}$$

$$\text{Adsorption capacity} : q = \frac{(C_0 - C)V}{m} \tag{2}$$

where C_0 is the initial concentration (mg L^{-1}), C is the equilibrium state or final concentration (mg L^{-1}), V is the volume of the solution (L), and m is the mass of the adsorbent (g).

The pH influence and the zero point of charge

The point of zero net charge, or isoelectric point (pH$_{PZC}$) of GO-NH_2-Fe_3O_4, was obtained to estimate in which pH the surface charge is positive—below ZPC—and negative—above ZPC. The point of zero charge (pH$_{PZC}$) of the adsorbent was determined according to the 12 points and salt addition method (Mahmood et al. 2011) by adding 1.0 mL of GO-NH_2-Fe_3O_4 suspension to several Erlenmeyer flasks. The solution volume with the adsorbent in each flask was 40 mL at 25 °C. A range of initial pH values (pH$_{initial}$) of the GO-NH_2-Fe_3O_4 suspensions was adjusted from 2.0 to 12.0 by adding small volumes of standard solutions of HCl and NaOH, 0.1 and 6.0 mol L^{-1}. The influence of the pH on the adsorption was evaluated through experiments ranging the initial pH from 2.0 to 12.0 and calculating the adsorption capacity per each initial solution pH.

Equilibrium studies and adsorption isotherms

Equilibrium studies were realized by ranging the MB concentration between 10 and 500 mg L^{-1}, where it was possible to determine the isotherm models which better described the adsorption mechanisms. Contact time was fixed at 20 min to ensure full equilibrium. Furthermore, the experiments were performed at 25 °C, 300 rpm and MB solution pH 12.0. After the experiments, all experimental data were plotted and the isotherms were fitted through mathematics software. Adsorption parameters, such as the equilibrium constant (K_L) and the maximum adsorption capacity (q_m), were obtained according to the model fitted to the experimental data.

The following models were tested to describe the adsorption process studied in this paper: the Langmuir, Freundlich, and Temkin. The Langmuir isotherm has been applied to many other real sorption process, and it has used to explain the sorption of dyes onto various adsorbents. The Langmuir adsorption isotherm follows the expression in Eq. 3:

$$\frac{q}{q_m} = \frac{K_L C}{1 + K_L C} \tag{3}$$

where q_m is the maximum adsorption capacity or the adsorption capacity when the system achieves the equilibrium (mg g^{-1}), K_L is the equilibrium constant (L mg^{-1}), C is the adsorbate concentration (mg L^{-1}), and q is the adsorption capacity for each concentration (mg g^{-1}).

The separation factor (R_L) is a dimensionless term which indicates the behavior of adsorption isotherm (Bozorgi et al. 2018; Ai et al. 2011; McCabe et al. 2005). According to Talebi et al. (2017), R_L values examine the types of isotherm: irreversible isotherm ($R_L = 0$), favorable isotherm ($0 < R_L < 1$), linear isotherm ($R_L = 1$), and unfavorable isotherm ($R_L > 1$). R_L values are given by Eq. 4:

$$R_L = \frac{1}{1 + K_L C_0} \tag{4}$$

where K_L is the Langmuir equilibrium constant (L g^{-1}) and C_0 is the highest initial concentration used at equilibrium studies (mg L^{-1}).

Freundlich's model assumes a non-uniform distribution of the adsorption energy over the adsorbent's heterogeneous surface (Araujo et al. 2018). The Freundlich mathematical model can be shown by Eq. 5:

$$q = K_F C^{1/n} \tag{5}$$

where K_F is the Freundlich constant (L mg^{-1}), $1/n$ is the factor of heterogeneity, C is the solution concentration, and q is the adsorption capacity.

The Temkin isotherm is widely used for adsorption systems of high concentrations and takes into account the adsorbent-adsorbate interactions and the uniform distribution of binding energy. Moreover, the heat of adsorption of all the molecules in the layer would decrease linearly with sorption capacity (Khan et al. 2015). The Temkin model is given by Eq. 6.

$$q = \frac{RT}{b_T} \ln(a_T C) \tag{6}$$

where a_T is the binding constant at the equilibrium (L mol^{-1}), b_T is the Temkin constant, R is the universal constant of the perfect gases (8.314 J K^{-1} mol^{-1}), and T is the environmental temperature, in which the experiment is performed (K).

Adsorption kinetics

For the kinetic study, aliquots of 25 mL of MB solution and the initial concentration (C_0) of 20 mg·L^{-1} were contacted with 1.0 mL of GO-NH$_2$-Fe$_3$O$_4$ suspension at a stirring speed of 300 rpm. The contact time ranged from 1 to 120 min. The experiments were conducted at 25 °C, 1 atm, and pH 12.0. To obtain the adsorption kinetic parameters (adsorption kinetic constant, k_f, k_s, and k_{ID}), the data were modeled using the non-linear fit provided by a mathematical software. Data modeling was performed according to Lagergren pseudo-first-order (PFO), Ho pseudo-second-order (PSO), and intraparticle diffusion (IPD) models, given by Eqs. 7, 8, and 9, respectively (Bozorgi et al. 2018; Lagergren 1898; Ho and McKay 2000).

$$q_t = q_e \left(1 - e^{-k_f t}\right) \tag{7}$$

where q_t is the adsorption capacity obtained at each time (mg g^{-1}), q_e is the adsorption capacity at the equilibrium state (mg g^{-1}), k_f is the pseudo-first-order adsorption rate constant (min^{-1}), and t is the contact time (min).

$$q_t = \frac{k_S q_e^2 t}{(1 + k_s q_e t)} \tag{8}$$

where k_s is the pseudo-second-order adsorption rate constant (g mg^{-1} min^{-1}).

Intraparticle diffusion model is given by the Eq. 9. This model is usually employed to describe the adsorption inside the pores of the adsorbent, neglecting the external mass transfer resistances to the adsorbent particles (McCabe et al. 2005).

$$q_t = k_{ID} t^{1/2} + k_0 \tag{9}$$

where k_{ID} is the intraparticle diffusion rate coefficient (L mol^{-1}), while k_0 is a constant related to the resistance to the diffusion (mg g^{-1}).
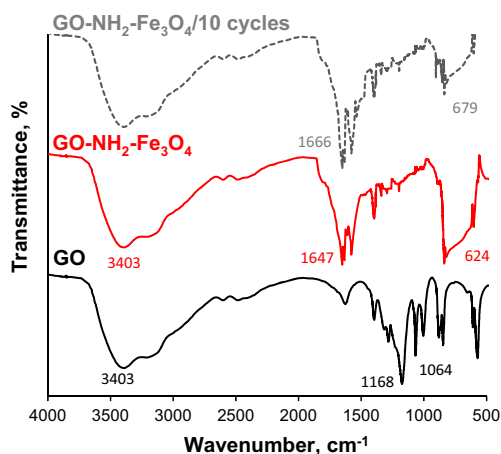
Fig. 1 FTIR spectra of GO, GO-NH$_2$-Fe$_3$O$_4$ and GO-NH$_2$-Fe$_3$O$_4$ after 10 MB adsorption-desorption cycles

Recyclability experiments

Adsorbent regeneration experiments were performed to evaluate losses in its adsorption performance after several cycles of adsorption-desorption. After MB adsorption at experimental conditions described in the batch mode adsorption section, GO-NH$_2$-Fe$_3$O$_4$ was separated from the MB solution by centrifugation and washed three times with distilled water to remove the non-adsorbed MB. After that, the sample was

transferred to a flask with 25 mL of distilled water in an incubator Shaker model Marconi MA-420 (Brazil) set in 65 °C, in agreement with some works in the literature, which reported desorption of dyes and other organic pollutants, such as pesticides and aromatic compounds, at higher temperatures than adsorptive process (Chen et al. 2016; Grajek 2000). Moreover, desorption experiments were performed at 300 rpm for 1 h and neutral pH ($\sim$ 7.00).

Results and discussion

Characterization of GO and GO-NH$_2$-Fe$_3$O$_4$

Figure 1 shows the FTIR spectra for GO and GO-NH$_2$-Fe$_3$O$_4$ and exhibited the characteristic peaks at 1632.5 cm^{-1}, attributed to the GO carbonyl (–C=O) stretching vibration; the broad band between at 3427 and 3250 cm^{-1} is referent to the O–H stretching vibration of the carboxylic acids groups of GO (Zhang et al. 2015), and this band was also revealed at GO-NH$_2$-Fe$_3$O$_4$ spectrum. However, bands with medium intensity between 3300 and 3500 cm^{-1} might be attributed to the presence of amine groups (–NH stretching vibration) on the sorbent surface. In the spectrum of GO-NH$_2$-Fe$_3$O$_4$, the peak at 580 cm^{-1} is attributed to the Fe–O bond vibration of Fe$_3$O$_4$
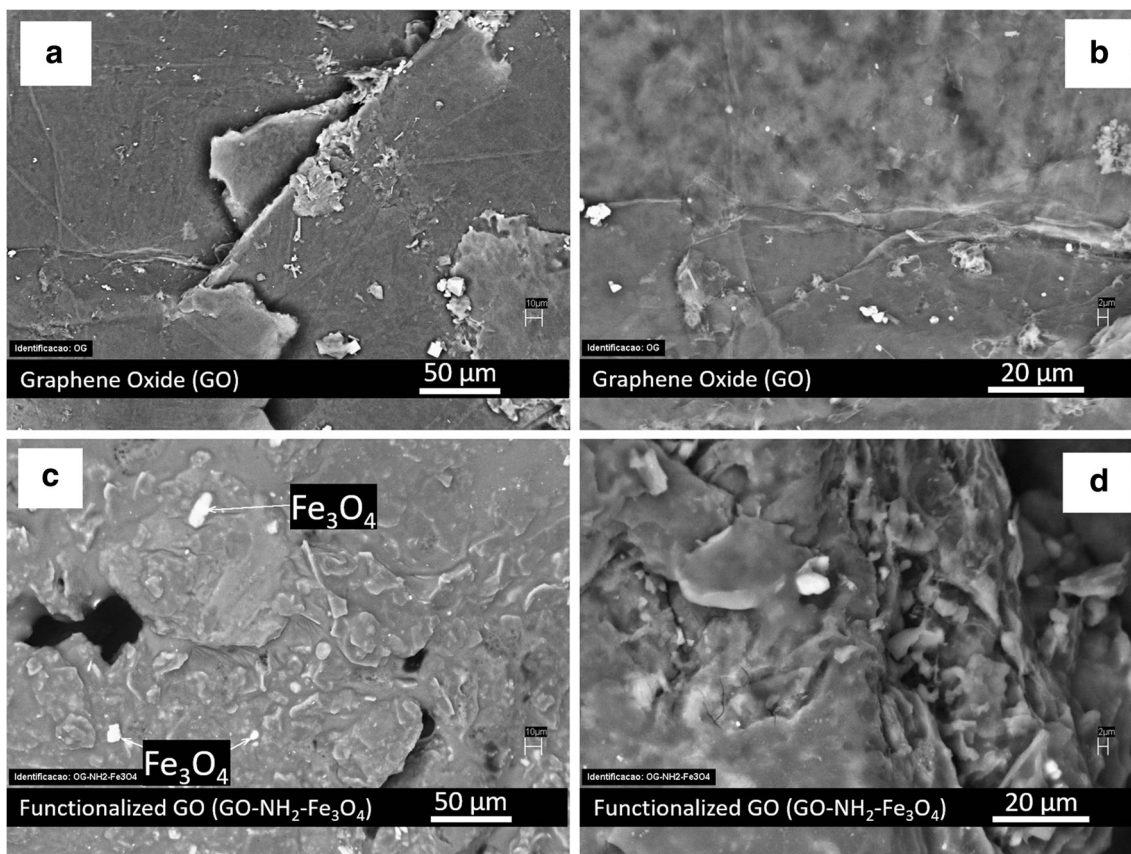

Fig. 2 SEM microscopy images for **(a)** GO ×500, **(b)** GO ×3000, **(c)** GO-NH$_2$-Fe$_3$O$_4$ ×500, **(d)** GO-NH$_2$-Fe$_3$O$_4$ ×3000

nanoparticles in the sorbent (Guo et al. 2015). The peak at 1572.5 cm^{-1} is caused by the stretching vibration and bending vibration of N–H bond, which is regarded to the presence of amino groups on the surface of the functionalized graphene (Zhao et al. 2016). Additionally, the intense peak at 1658.0 cm^{-1} might be attributed to amide groups, as a consequence of parallel reactions during the functionalization synthesis.

Morphological structures of GO and GO-NH$_2$-Fe$_3$O$_4$ are depicted in Fig. 2. It is possible to visualize the overlap of some folded layers and wrinkles between them. In addition, some clear spots of aggregation, with a much higher overall roughness, can be seen on the GO-NH$_2$-Fe$_3$O$_4$ surface (Fig. 2c, d), as compared to the GO sample (Fig. 2a, b). The EDX analyses indicated the presence of Fe in several spots on the GO-NH$_2$-Fe$_3$O$_4$ surface (see marks on Fig. 2c), confirming the successful incorporation of magnetite (Fe$_3$O$_4$) nanoparticles onto the GO surface.

Graphite powder, GO, and GO-NH$_2$-Fe$_3$O$_4$ were characterized by XRD (Fig. 3a) and compared to the standard of graphite (JCPDS 75-2078, 3347 Å). For graphite, the peaks equal to 26.5° and 54.6°, diffraction planes (002) and (004), referring to the basal planes of the graphene, were observed in addition to the plane (101) in 44.5°. All these peaks are characteristic of three-dimensional crystalline graphite. The plane (002) is quite narrow and intense. The spectra of the synthesized GO and GO-NH$_2$-Fe$_3$O$_4$ show the same behavior (Fig. 3a), and there is an indication of an amorphous band characteristic of non-crystalline materials, such as few layer graphene; however, it is possible to notice the presence of small peaks. Amorphous traces of the peak related to plane (002) were shifted to 25.5° and suggest that the oxidation of graphite structure was not sufficient to oxidize 100% of the layers. For the GO-NH$_2$-Fe$_3$O$_4$, there is also an indication of a small peak, still related to the plane (002), which was shifted to 11° and is characteristic of interplanar distances of ~ 0.8 nm (Stephan et al. 1994). This distance is greater than the
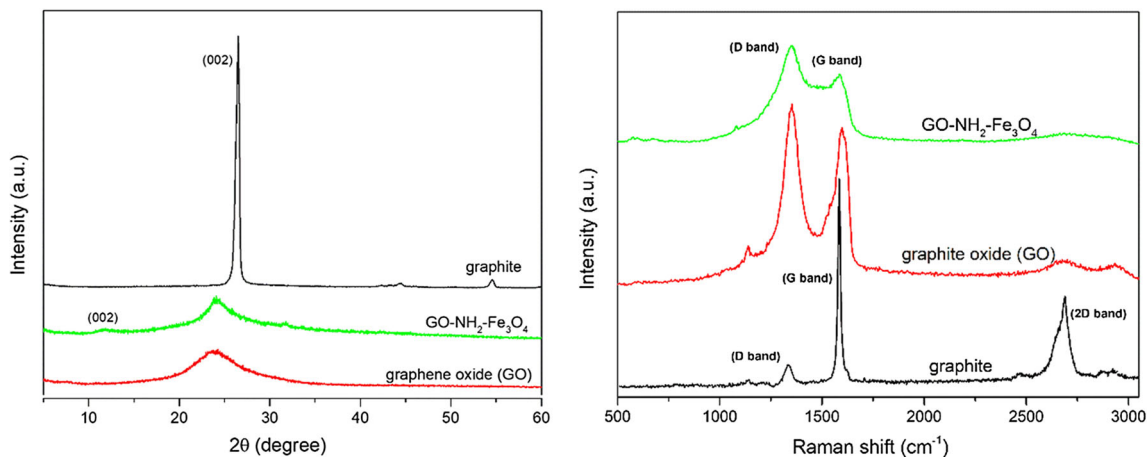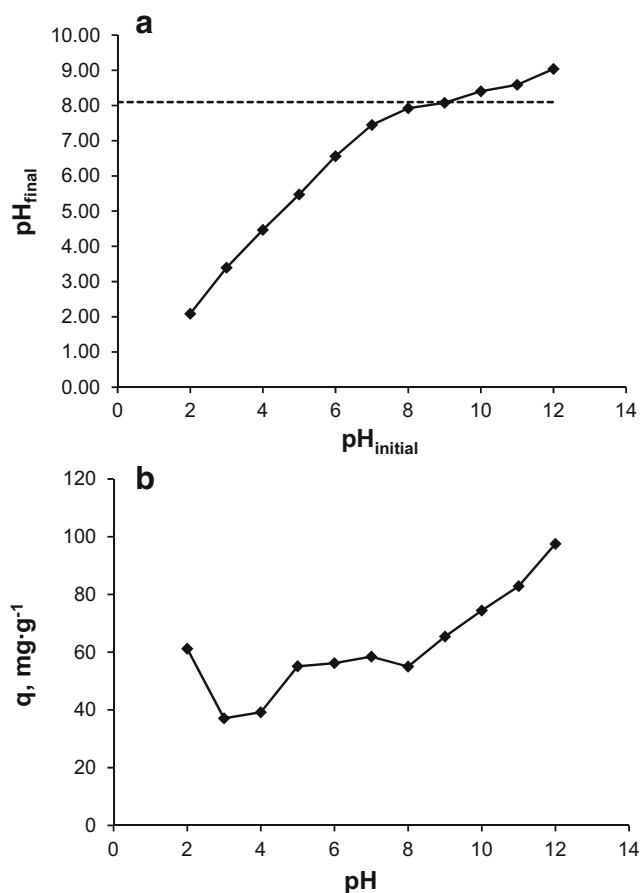
Fig. 4 (a) Point of zero charge of GO-NH$_2$-Fe$_3$O$_4$. (b) Effect of pH in the MB adsorption

separation of the graphene sheets (0.34 nm); therefore, it is suggested the formation of functional groups, like phenolic, amino, ferritic groups, and hydroxyl between the graphite nanolayers during their functionalization.

Raman spectra of GO, GO-NH$_2$-Fe$_3$O$_4$, and graphite powder are compared in Fig. 3b. The spectra of all carbon systems have a set of characteristic bands; the main bands are the D
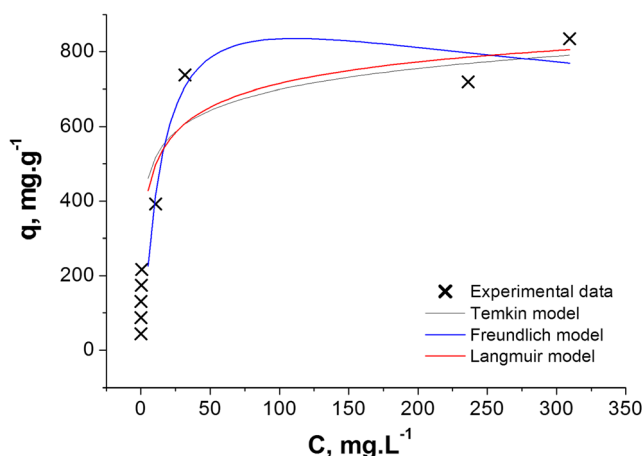
Fig. 3 XRD and Raman patterns for graphite precursor, GO, and GO-NH$_2$-Fe$_3$O$_4$

Fig. 5 Isotherm for adsorption of MB onto OG-NH$_2$-Fe$_3$O$_4$. Experiments performed at 300 rpm, 25 mL, and pH 12.0
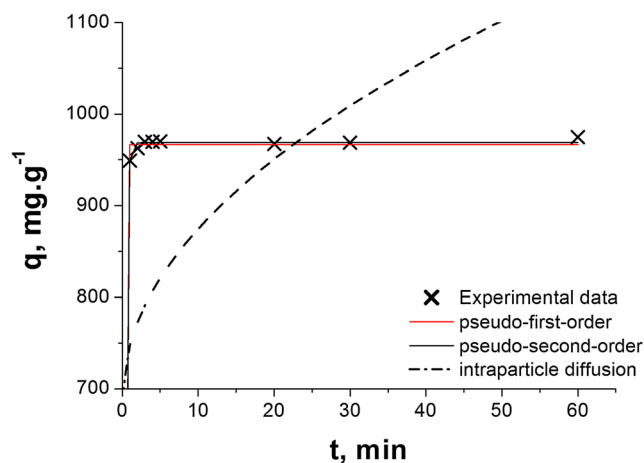

Fig. 6 Kinetic experimental data of the adsorption of MB by GO-NH$_2$-Fe$_3$O$_4$ and PSO model. Experiments performed at 25 °C, 25 mL, pH 12.0, and 300 rpm

band (~ 1360 cm^{-1}) and G band (~ 1560 cm^{-1}), as well as few other second-order harmonics. According to Ferrari, G band is due to the stretching movement of the sp^2 bonds between carbon atoms of the basal 2D plane, which reflects the planar crystalline structure of the graphite/graphene materials. Band D is due to Raman scattering in the discontinuity zone, which reflects disordered structures. Such structures include defects, boundaries of crystals, breaking of symmetry, etc. The most prominent second-order harmonic, around 2700 cm^{-1}, is called the 2D band and reflects the stacking structure of the graphene sheets along the c axis (perpendicular) (Ferrari et al. 2006). According to analysis, the two most intense features for graphite powder are, as expected, the G peak at ~ 1575 cm^{-1} and the 2D peak at ~ 2681 cm^{-1}. For the oxidized (GO) and functionalized (GO-NH$_2$-Fe$_3$O$_4$), no clear 2D peak can be identified. Chemical modifications like oxidation/functionalization can lead to severe structural damage to the surface of these materials, introducing defects, which could include residual carboxylic acids, epoxides, and amino and ferritic groups, that may disrupt the band structure. The broadness and high intensity of the defect D peak (small in graphite powder precursor) for these samples confirm this assumption (Ghislandi et al. 2015).

pH$_{PZC}$ and effect of pH in adsorption

The point of zero charge analysis showed that the pH$_{PZC}$ was 8.2 (Fig. 4a). The evaluation of pH influence on the adsorption (Fig. 4b) showed that the cationic MB better adsorb at basic pH (12.00), above pH$_{PZC}$. These results evidenced that, beyond π-π interactions, electron donor-receptor relationships between MB and GO-NH$_2$-Fe$_3$O$_4$ structures are also present in the adsorption mechanism. Hence, all the further experiments were conducted at pH 12.0 to favor adsorbate-adsorbent electronic interactions on GO-NH$_2$-Fe$_3$O$_4$ surface.

Equilibrium studies

By the adsorption isotherm depicted in Fig. 5, MB adsorption presented a downward concavity and separation factor (R_L) 0.005, characterizing a favorable behavior ($0 < R_L < 1$) (Bozorgi et al. 2018; McCabe et al. 2005). Mathematical modeling showed that Langmuir model (Eq. 3) better fitted the experimental data in comparison to other models and showed satisfactory coefficient of determination, 0.936. Incidentally, according to Ruthven (1984), Langmuir model
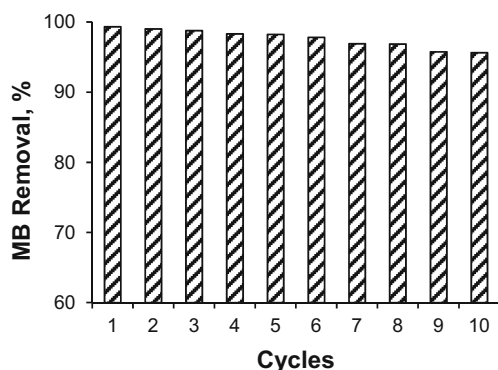
Table 1 Equilibrium and kinetic parameters for the adsorption of MB by GO-NH$_2$-Fe$_3$O$_4$

Equilibrium models					
Langmuir		Freundlich		Temkin	
q_m, mg g^{-1}	1047.81	K_f, mg$^{1-1/n}$ L$^{1/n}$ g^{-1}	15.20	a_T, L mol^{-1}	55.96
K_L, L mg^{-1}	3.65×10^{-1}	N	2.31	b_T	30.58
R_L	5.45×10^{-3}				
R^2	0.936	R^2	0.802	R^2	0.917
Kinetic models					
Pseudo-first-order		Pseudo-second-order		Intraparticle diffusion	
k_F, min^{-1}	3.86	k_S, g mg^{-1} min^{-1}	3.17×10^{-2}	k_{ID}, L mol^{-1}	58.18
q_e, mg g^{-1}	969.00	q_e, mg g^{-1}	966.39	k_0, mg g^{-1}	690.42
R^2	0.991	R^2	0.999	R^2	0.201

Fig. 7 MB adsorption-desorption cycles onto GO-NH$_2$-Fe$_3$O$_4$; experiments performed at 1 h (regeneration time), 65 °C, 300 rpm; MB adsorption at pH 12.0

is best representative for monolayer adsorption and homogeneous adsorption systems. Langmuir maximum adsorption capacity (q_m) and sorption equilibrium constant (K_L) of MB removal onto GO-NH$_2$-Fe$_3$O$_4$ were 1047.81 mg g^{-1} and 3.65×10^{-1} L mg^{-1}, respectively. Table 2 presents a comparative study of the adsorption efficiency, equilibrium and kinetics models and recyclability of GO-NH$_2$-Fe$_3$O$_4$ and other adsorbents found in the literature. GO-NH$_2$-Fe$_3$O$_4$ maximum adsorption capacity is more than twice the adsorption of MB onto GO (Araujo et al. 2018), and considerably higher than other nanocarbon-derived adsorbents found in the literature for the adsorption of dyes (Ganesan et al. 2018; Zhao et al. 2017; Carvallho et al. 2016). Furthermore, Temkin model (Eq. 6) was also tested for MB adsorption by GO-NH$_2$-Fe$_3$O$_4$, and its constants, obtained for the equilibrium process, a_T and b_T,

were 55.96 L mol^{-1} and 30.58 kJ mol^{-1}, respectively. Relatively lower values of b_T are an indicative of the Temkin isotherm that can be applied to explain the experimental equilibrium data, as verified in the availability of experimental data found in the literature (Araujo et al. 2018; Das et al. 2018; Wanjeri et al. 2018; Lingamdinne et al. 2018). Equilibrium parameters for every model evaluated in this study, as well as their coefficient of determination, can be seen in Table 1.

Adsorption kinetics

All experiments were carried out at MB solution pH 12.0. The kinetic modeling curves showed a fast adsorption process of the MB (Fig. 6), in which the equilibrium state was reached after 5 min, where experimental adsorption capacity was 969.84 mg g^{-1}. Rapid adsorption is an indicative of the physical nature of adsorption (Ruthven 1984; McCabe et al. 2005). After adjusting the experimental data according to the kinetic models expressed in Eqs. 3, 4, and 5, it was verified that the pseudo-second order model (Fig. 6) was fitted to the process, with a satisfactory coefficient of determination ($R^2 = 0.999$). Kinetic models evaluated and their parameters are reported in the Table 1. The pseudo-second-order model better fitted the adsorption, in which equilibrium adsorption capacity (q_e) and the PSO kinetic constant (k_s) were 966.39 mg g^{-1} and 3.17×10^{-2} g mg^{-1} min^{-1}. PSO lower adsorption rate represents a quick adsorptive process, which indicates that MB adsorption in this case occurs, preferably, on OG-NH$_2$-Fe$_3$O$_4$ surface, in

Table 2 Comparative study of dye adsorption by several carbonaceous nano-adsorbents found in the literature

Adsorbent	Adsorbate	q_m, mg g^{-1}	Isotherm model	Kinetic model	Predicted mechanism[a]	pH	Regen. cycles	Reference
GO	Methylene Blue	504.00	Temkin	PSO	Electrostatic inter., π-π	4.0–6.0	N/A	Araujo et al. (2018)
r-GO	Methylene Blue	144.90	Langmuir	PSO	Electrostatic inter.	8.0–12.0	N/A	Minitha et al. (2017)
Hemin-GO	Methylene Blue	99.20	N/A	PSO	π-π	9.0	5	Zhao et al. (2017)
GO	Rhodamine B	224.00	Temkin	IPD	π-π	4.0	7	Das et al. (2018)
Bi$_2$O$_3$-GO	Rhodamine B	320.00	Temkin	IPD	H-bond	4.0	N/A	Das et al. (2018)
Fe$_3$O$_4$-GO	Rhodamine B	39.65	Langmuir	PSO	π-π	3.0	8	Ganesan et al. (2018)
β-Cyclodextrin-Graphene	Methyl Orange	328.20	Langmuir	PSO	π-π	N/A	6	Tan and Hu (2017)
xGnP™ graphite nanoplatelets	Indosol SFGL Blue	24.95	BET	PSO	π-π	2.0–4.0	N/A	Carvallho et al. (2016)
xGnP™ graphite nanoplatelets	Drimaren HFRL Blue	50.66	BET	PSO	π-π	2.0	N/A	Carvallho et al. (2016)
Methylimidazolium-GO	Direct Red 80	501.30	Langmuir	PSO	Electrostatic inter.	12.0	4	Zambare et al. (2017)
GO-NH$_2$-Fe$_3$O$_4$	Methylene Blue	1047.81	Langmuir	PSO	Electrostatic inter., π-π	12.0	10	This work

PFO pseudo-first-order, *PSO* pseudo-second-order, *IPD* intraparticle diffusion

[a] Reported interactions which govern the adsorption

agreement with the theoretical information found in the literature (McCabe et al. 2005). Intraparticle diffusion model did not fit the experimental data ($R^2 = 0.201$), once the layered GO-NH$_2$-Fe$_3$O$_4$ does not have porous structure and the MB molecules stay in parallel with graphene basal plane, interacting with OH, NH$_2$, and other groups on its surface (Minitha et al. 2017). Moreover, the MB sorption kinetics onto graphene nanomaterials being fitted by PSO model suggest that adsorption was a function of boundary layer thickness and external mass transfer, without resistance to mass transfer within the pores of the adsorbent (Diraki et al. 2018).

Sorbent recyclability

GO-NH$_2$-Fe$_3$O$_4$ recyclability was evaluated at pH 12.0 (Fig. 7), and it was found that the sorbent efficiency remained 95.6% after 10 cycles. Moreover, there were no substantive loss in the MB removal efficiency through the adsorption/desorption cycles. Reported data evidenced that graphene-based nanomaterials ensure great adsorption capacity, mild operational conditions, and high recyclability; consequently, they can be described with no doubt as ecofriendly adsorbents. It is easily observed an outstanding recyclability of GO-NH$_2$-Fe$_3$O$_4$ in comparison to other graphene-based materials (Table 2), which may be employed for several types of water pollutants. By the collected data, GO-NH$_2$-Fe$_3$O$_4$ elevated adsorption capacity, fast adsorption, and high recyclability can be highlighted. Additionally, FTIR spectrum of GO-NH$_2$-Fe$_3$O$_4$ after 10 regeneration cycles (Fig. 1) showed no relevant changes in comparison to GO-NH$_2$-Fe$_3$O$_4$, which demonstrates that there were no losses or breakdown of functional groups and consequently proves that the regeneration of GO-NH$_2$-Fe$_3$O$_4$ was successfully performed.

Conclusions

The objective of this work was to evaluate the adsorption capability of the amino-functionalized graphene oxide as an adsorbent of textile dyes, using Methylene Blue as a reference dye. The oxidation of graphite to form GO sheets was confirmed by XRD and Raman characterization. Moreover, the visualization and successful functionalization of OG surface with NH$_2$-Fe$_3$O$_4$ was confirmed via FTIR and SEM analyses. Kinetic experiments showed that the equilibrium state in the adsorption process occurs quickly, within 5 min, which points to a tendency of physisorption; moreover, kinetic pseudo-second-order better fitted the experimental data. Equilibrium studies showed that the Langmuir isotherm was the best fit for the experimental data. Thereafter, GO-NH$_2$-Fe$_3$O$_4$ reached an elevated maximum adsorption capacity, double of the GO as adsorbent of MB, and substantively higher than other graphene-derived adsorbents. In view of the outstanding

adsorption capacity and elevated recyclability in comparison to several adsorbents found in the literature, there is a good perspective for the application of amino-functionalized graphene oxide as an ecofriendly adsorbent of reactive or direct textile dyes, widely used in textile industries.

References

Ai L, Zhang C, Chen Z (2011) Removal of methylene blue from aqueous solution by a solvothermal-synthesized graphene/magnetite composite. J Hazard Mater 192:1515–1524. https://doi.org/10.1016/j.jhazmat.2011.06.068

Al-Qodah Z, Lafi WK, Al-Anber Z, Al-Shannag M, Harahsheh A (2007) Adsorption of methylene blue by acid and heat treated diatomaceous silica. Desalination 217:212–224. https://doi.org/10.1016/j.desal.2007.03.003

Araujo CMB, Assis Filho RB, Baptisttella AMS, Nascimento GFO, da Costa GRB, Carvalho MN, Ghislandi M, da Motta Sobrinho MA (2018) Systematic study of graphene oxide production using factorial design techniques and its application to the adsorptive removal of methylene blue dye in aqueous medium. Mater Res Express 5(6). https://doi.org/10.1088/2053-1591/aacb51

Bozorgi M, Abbasizadeh S, Samani F, Mousavi SE (2018) Performance of synthesized cast and electrospun PVA/chitosan/ZnO-NH2 nano-adsorbents in single and simultaneous adsorption of cadmium and nickel ions from wastewater. Environ Sci Pollut Res 25:17457–17472. https://doi.org/10.1007/s11356-018-1936-z

Carvallho MN, da Silva KS, Sales DCS, Freire EM, Sobrinho MAM, Ghislandi MG (2016) Dye removal from textile industrial effluents by adsorption on exfoliated graphite nanoplatelets: kinetic and equilibrium studies. Water Sci Technol 73(9):2189–2198. https://doi.org/10.2166/wst.2016.073

Cha C, Shin SR, Annabi N, Dokmeci MR, Khademhosseini A (2013) Carbon-based nanomaterials: multifunctional materials for biomedical engineering. ACS Nano 7(4):2891–2897. https://doi.org/10.1021/nn401196a

Chen L, Li Y, Hu S, Sun J, Du Q, Yang X, Ji Q, Wang Z, Wang D, Xia Y (2016) Removal of methylene blue from water by cellulose/graphene oxide fibres. J Exp Nanosci 11(14):1156–1170. https://doi.org/10.1080/17458080.2016.1198499

Das TR, Patra S, Madhuri R, Sharma PK (2018) Bismuth oxide decorated graphene oxide nanocomposites synthesized via sonochemical assisted hydrothermal method for adsorption of cationic organic dyes. J Colloid Interface Sci 509:82–93. https://doi.org/10.1016/j.jcis.2017.08.102

Diraki A, Mackey H, McKay G, Abdala A (2018) Removal of oil from oil–water emulsions using thermally reduced graphene and graphene nanoplatelets. Chem Eng Res Des 137:47–59. https://doi.org/10.1016/j.cherd.2018.03.030

Ferrari AC, Meyer J, Scardaci V, Casiraghi C, Lazzeri M, Mauri F, Piscanec S, Jiang D, Novoselov KS, Roth S, Geim AK (2006) Raman spectrum of graphene and graphene layers. Phys Rev Lett 97(18):187401. https://doi.org/10.1103/PhysRevLett.97.187401

Ganesan V, Louis C, Damodaran SP (2018) Graphene oxide-wrapped magnetite nanoclusters: a recyclable functional hybrid for fast and highly efficient removal of organic dyes from wastewater. J Environ

Chem Eng 6(2):2176–2190. https://doi.org/10.1016/j.jece.2018.03.026

Georgakilas V, Tiwari JN, Kemp KC, Perman JA, Bourlinos AB, Kim KS, Zboril R (2016) Noncovalent functionalization of graphene and graphene oxide for energy materials, biosensing, catalytic, and biomedical applications. Chem Rev 116:5464–5519. https://doi.org/10.1021/acs.chemrev.5b00620

Ghislandi M, Tkalya E, Alekseev A, Koning C, de With G (2015) Electrical conductive behavior of polymer composites prepared with aqueous graphene dispersions. Appl Mater Today 1:88–94. https://doi.org/10.1016/j.apmt.2015.11.001

Grajek H (2000) Regeneration of adsorbents by the use of liquid, subcritical and supercritical carbon dioxide. Adsorpt Sci Technol 18(4):347–371. https://doi.org/10.1260/0263617001493486

Grima JN, Winczewski S, Mizzi L, Grech MC, Cauchi R, Gatt R, Attard D, Wojciechowski KW, Rybicki J (2015) Tailoring graphene to achieve negative Poisson's ratio properties. Adv Mater 27:1455–1459. https://doi.org/10.1002/adma.201404106

Guo LQ, Ye PR, Wang J, Fu FF, Wu ZJ (2015) Three-dimensional Fe3O4-graphene macroscopic composites for arsenic and arsenate removal. J Hazard Mater 298:28–35. https://doi.org/10.1016/j.jhazmat.2015.05.011

Ho YS, Mckay G (2000) The kinetics of sorption of divalent metal ions onto sphagnum moss peat. Water Res 34(3):735–742. https://doi.org/10.1016/S0043-1354(99)00232-8

Hu J, Deng W, Chen D (2017) Ceria hollow spheres as an adsorbent for efficient removal of acid dye. ACS Sustain Chem Eng 5(4):3570–3582. https://doi.org/10.1021/acssuschemeng.7b00396

Hummers WS, Offeman RE (1958) Preparation of graphitic oxide. J Am Chem Soc 80(6):1339–1339. https://doi.org/10.1021/ja01539a017

Khan TA, Chaudhry SA, Ali I (2015) Equilibrium uptake, isotherm and kinetic studies of Cd(II) adsorption onto iron oxide activated red mud from aqueous solution. J Mol Liq 202:165–175. https://doi.org/10.1016/j.molliq.2014.12.021

Kuila T, Bose S, Mishra AK, Khanra P, Kim NH, Lee JH (2012) Chemical functionalization of graphene and its applications. Prog Mater Sci 57:1061–1105. https://doi.org/10.1016/j.pmatsci.2012.03.002

Lagergren S (1898) About the theory of so-called adsorption of soluble substances. Kungliga Svenska Vetenskapsakademiens Handlingar (in Swedish)

Lazarevic-Pasti T, Anicijevic V, Baljozovic M, Vasic Anicijevic D, Gutic S, Vasic V, Skorodumova NV, Pasti IA (2018) Environ Sci Nano (just accepted). https://doi.org/10.1039/C8EN00171E

Lingamdinne LP, Koduru JR, Chang Y-Y, Karri RR (2018) Process optimization and adsorption modeling of Pb(II) on nickel ferrite-reduced graphene oxide nano-composite. J Mol Liq 250:202–211. https://doi.org/10.1016/j.molliq.2017.11.174

Mahmood T, Saddique MT, Naeem A, Westerhoff P, Mustafa S, Alum A (2011) Comparison of different methods for the point of zero charge determination of NiO. Ind Eng Chem Res 50:10017–10023. https://doi.org/10.1021/ie200271d

McCabe WL, Smith JC, Harriott P (2005) Unit operations of chemical engineering, 5th edn. McGraw-Hill, Nova York

Minitha CR, Lalitha M, Jeyachandran YL, Senthil Kumar L, Kumar RTR (2017) Adsorption behaviour of reduced graphene oxide towards cationic and anionic dyes: co-action of electrostatic and π-π interactions. Mater Chem Phys 194:243–252. https://doi.org/10.1016/j.matchemphys.2017.03.048

Novoselov KS, Geim AK, Morozov SV, Jiang D, Zhang Y, Dobonos SV, Griorieva IV, Firsov AA (2004) Electric field effect in atomically thin carbon films. Science 306:666–669. https://doi.org/10.1126/science.1102896

Ruthven DM (1984) Principles of adsorption and adsorption processes. Wiley, New York

Shaban M, Abukhadra MR, Khan AAP, Jibali BM (2018) Removal of Congo red, methylene blue and Cr(VI) ions from water using natural serpentine. J Taiwan Inst Chem Eng 82:102–116. https://doi.org/10.1016/j.jtice.2017.10.023

Stephan O, Ajayan P, Colliex C, Redlich P, Lambert JM, Bernier P, Lefin P (1994) Doping graphitic and carbon nanotube structures with boron and nitrogen. Science 266(5191):1683–1685. https://doi.org/10.1126/science.266.5191.1683

Talebi M, Abbasizadeh S, Keshtkar AR (2017) Evaluation of single and simultaneous thorium and uranium sorption from water systems by an electrospun PVA/SA/PEO/HZSM5 nanofiber. Process Saf Environ Prot 109:340–356. https://doi.org/10.1016/j.psep.2017.04.013

Tan P, Hu Y (2017) Improved synthesis of graphene/β-cyclodextrin composite for highly efficient dye adsorption and removal. J Mol Liq 242:181–189. https://doi.org/10.1016/j.molliq.2017.07.010

Wang Z, Xue M, Huang K, Liu Z (2011) In: Hauser P (ed) Textile dyeing wastewater treatment, advances in treating textile effluent. Intech Open, Shanghai

Wanjeri VWO, Sheppard CJ, Prinsloo ARE, Ngila JC, Ndungu PG (2018) Isotherm and kinetic investigations on the adsorption of organophosphorus pesticides on graphene oxide based silica coated magnetic nanoparticles functionalized with 2-phenylethylamine. J Environ Chem Eng 6:1333–1346. https://doi.org/10.1016/j.jece.2018.01.064

World Bank Group (2007) Environmental, health, and safety guidelines for textile manufacturing. IFC – International Finance Coorporation, Washington

Yang RT (2003) Adsorbents: fundamentals and applications. Wiley, Hoboken

Yu L, Wang L, Xu W, Chen L, Fu M, Wu J, Ye D (2017) Adsorption of VOCs on reduced graphene oxide. J Environ Sci 67:171–178. https://doi.org/10.1016/j.jes.2017.08.022

Yusuf M, Elfghi FM, Zaidi SA, Abdullah EC, Khan MA (2015) Applications of graphene and its derivatives as an adsorbent for heavy metal and dye removal: a systematic and comprehensive overview. RSC Adv 5:50392–50420. https://doi.org/10.1039/C5RA07223A

Zambare R, Song X, Bhuvana S, Prince JSA, Nemade P (2017) Ultrafast dye removal using ionic liquid−graphene oxide sponge. ACS Sustain Chem Eng 5:6026–6035. https://doi.org/10.1021/acssuschemeng.7b00867

Zhang FR, Song YW, Song S, Zhang RJ, Hou WG (2015) Synthesis of magnetite-graphene oxide-layered double hydroxide composites and applications for the removal of Pb(II) and 2,4-dichlorophenoxyacetic acid from aqueous solutions. ACS Appl Mater Interfaces 7:7251–7263. https://doi.org/10.1021/acsami.5b00433

Zhang Z, Gao T, Si S, Liu Q, Wu Y, Zhou G (2018) One-pot preparation of p(TA-TEPA)-PAM-rGO ternary composite for high efficient Cr(VI) removal from aqueous solution. Chem Eng J 343:207–216. https://doi.org/10.1016/j.cej.2018.02.126

Zhao D, Gao X, Wu C, Xie R, Feng S, Chen C (2016) Facile preparation of amino functionalized graphene oxide decorated with Fe3O4 nanoparticles for the adsorption of Cr(VI). Appl Surf Sci 384:1–9. https://doi.org/10.1016/j.apsusc.2016.05.022

Zhao Y, Zhang Y, Liu A, Wei Z, Liu S (2017) Construction of three-dimensional hemin-functionalized graphene hydrogel with high mechanical stability and adsorption capacity for enhancing photodegradation of methylene blue. ACS Appl Mater Interfaces 9(4):4006–4014. https://doi.org/10.1021/acsami.6b10959

Zhu H, Chen T, Liu J, Li D (2018) Adsorption of tetracycline antibiotics from an aqueous solution onto graphene oxide/calcium alginate composite fibers. RSC Adv 8:2616–2621. https://doi.org/10.1039/c7ra11964j